ELSEVIER

Journal of Nuclear Materials 304 (2002) 21–28

journal of nuclear materials

www.elsevier.com/locate/jnucmat

Oxidation behavior of modified SUS316 (PNC316) stainless steel under low oxygen partial pressure

I. Sato [a,*], M. Takaki [b], T. Arima [b], H. Furuya [b], K. Idemitsu [b], Y. Inagaki [b], M. Momoda [b], T. Namekawa [a]

[a] *Japan Nuclear Fuel Cycle Development Institute, O-arai Engineering Center, 4002 Narita-cho, O-arai-machi, Ibaraki 311-1393, Japan*
[b] *Department of Nuclear Engineering, Faculty of Engineering, Kyushu University, 6-10-1 Hakozaki, Fukuoka 812-8581, Japan*

Received 25 June 2001; accepted 18 April 2002

Abstract

Oxidation behaviors of modified SUS316 (PNC316) and SUS316 stainless steels were investigated under the low oxygen partial pressure of $10^{-31} - 10^{-22}$ atm at 600–800 °C. Oxygen uptake by these materials parabolically increased with time, and the kinetic rate constants depended on both oxygen partial pressure and temperature. Thus, semi-empirical equations of the parabolic rate constants were obtained to be $2.70 \times 10^4 \exp(-109/RT)P_{O_2}^{0.279}$ for PNC316 and $9.23 \times 10^4 \exp(-98/RT)P_{O_2}^{0.313}$ for SUS316. For the duplex layer formed under the low oxygen partial pressure, the inner layer consisted of such oxides as Cr_2O_3 and $FeCr_2O_4$, while the outer layer consisted of non-oxidized α-Fe. Furthermore, oxidation along the grain boundaries was observed for samples oxidized for a long time. From the point of view of fuel cladding chemical interaction evaluation at high burn-up fuel for fast reactors, it is interesting that formation of non-oxidized α-Fe was observed under the low oxygen partial pressure.

PACS: 28.41.T; 81.65.M

1. Introduction

A fast reactor oxide fuel, which is a mixed-oxide fuel (MOX) consisting of solid solution of UO_2 and PuO_2, is expected to be irradiated to a burn-up of more than 20 at.% [1]. Therefore, the O/M ratio of MOX is generally designed to be lower than that of light water reactor fuels in order to lead to retardation of oxidation and/or corrosion of the inner surface of cladding. In other words, the oxygen partial pressure seems to be extremely low at the initial stage of burn-up [2–4]. Oxidation of the cladding, which is the major reaction until enough amount of corrosive fission products (FPs) is accumulated, is important for analyzing the fuel cladding chemical interaction (FCCI) as well as the oxygen balance in the closed fuel pin in terms of excess oxygen buildup with fissions, oxidation of FPs, stoichiometry of fuel and so on.

There have been a few studies so far on the oxidation behavior of stainless steels under low oxygen partial pressure. Bannet observed that oxidation of stainless steel was dependent on oxygen partial pressure under the Ar–O_2 atmosphere [5]. Noda evaluated effects of impurities on the oxidation behavior under He gas atmosphere [6]. However, these works revealed only qualitative aspects of oxidation of stainless steels under low oxygen partial pressure. Saito reported quantitative analyses using Mo/MoO_2 or NbO_2/Nb_2O_5 oxygen buffer, in which the oxidation kinetic constant was a function of oxygen partial pressure to the *n*th power [7]. However, in order to more systematically estimate the oxygen balance in fuel pins, it is needed to perform the oxidation experiments under more widely and/or lower oxygen partial pressures.

* Corresponding author. Tel.: +81-29 267 4141; fax: +81-29 266 3714.
E-mail address: isato@oec.jnc.go.jp (I. Sato).

0022-3115/02/$ - see front matter
PII: S0022-3115(02)00872-3

The austenitic stainless steel of PNC316, so-called 'modified SUS316', is the cladding material used in the fast reactor 'MONJU', and has been loaded in the experimental fast reactor 'JOYO' [8]. This material exhibits good characteristics in creep rupture strength and swelling resistance due to optimized added minor elements such as Ti, Nb, P etc. and heat treatments for 316 type stainless steel.

In this work, dependence of the oxidation rate of PNC316 on both the oxygen partial pressure and temperature has been measured by using a carrier gas extract oxygen analyzer. And the oxygen partial pressure was controlled by changing the ratio of pressures of H_2 and H_2O gas components. In addition, X-ray diffractometry (XRD) and electron probe X-ray microanalysis (EPMA) were performed on the oxidized samples. On the basis of data obtained in these measurements, the oxidation behavior of PNC316 under low oxygen partial pressure was evaluated in detail.

2. Experimental

The specimens used in this oxidation experiment were cut from billet into plates of 5 $mm^w \times 5$ $mm^l \times 0.5$ mm^t. The elemental compositions of PNC316 and SUS316 are listed in Table 1. PNC316 contains small amounts of Ti and Nb unlike SUS316. The specimen surfaces were polished on abrasive papers and then subsequently finished by alumina buffing.

The schematic view of the experimental apparatus is shown in Fig. 1. The oxidation experiments were performed in the temperature range of 600–800 °C under the oxygen partial pressure between 10^{-31} and 10^{-22} atm. The oxygen partial pressure was controlled by changing the ratio of pressures of H_2 and H_2O gas components in Ar carrier gas. Ar and Ar/H_2 gas were separately supplied to the oxidation apparatus. Each gas was purified by ethanol + dry ice (∼−72 °C), and subsequently was deoxidized by Ti granules heated at 800 °C. Then, for

Table 1
Elemental compositions of PNC316 and SUS316 stainless steels (wt%)

	C	Si	Mn	P	Ni	Cr	Mo	B	Ti	Nb	Fe
PNC316	0.06	0.79	1.68	0.029	13.80	16.55	2.55	0.0045	0.079	0.076	Bal.
SUS316	0.052	0.43	1.04	0.023	13.69	16.46	2.51	0.0017	–	–	Bal.

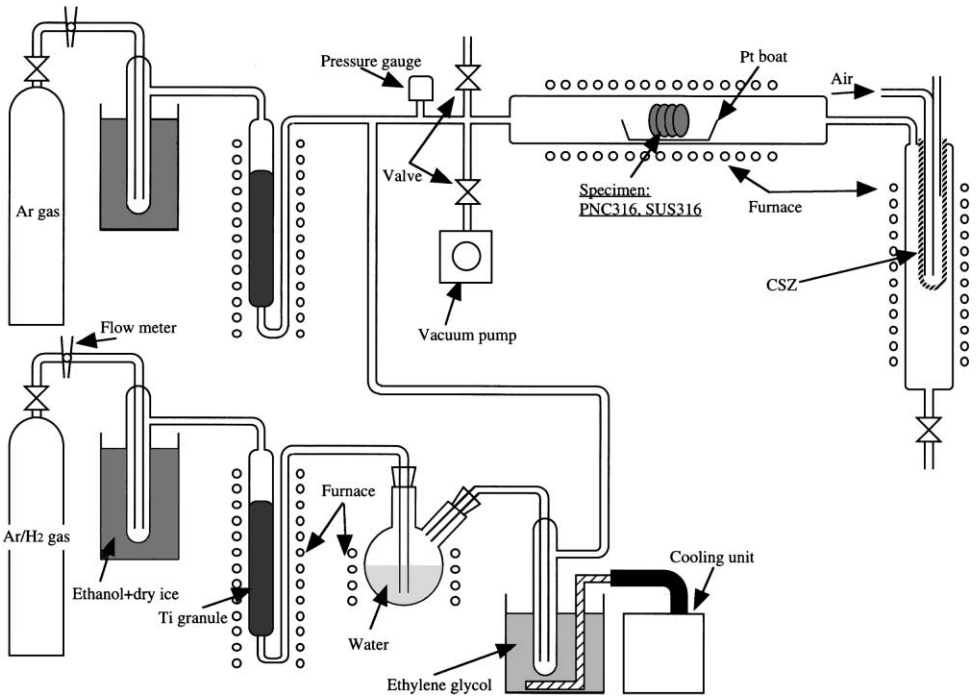

Fig. 1. Schematics of experimental apparatus for oxidation under the low oxygen partial pressure.

purified Ar gas, steam generated from hot water was condensed in a dew controller to get the expected partial pressure of H_2O vapor. Finally, Ar/H_2 and Ar/H_2O gases were mixed with each other, and were led to the reaction system. Thus, the oxygen partial pressure was controlled to the equilibrium oxygen partial pressure of each H_2–H_2O gas mixture. The value of oxygen partial pressure was measured with a calcia-stabilized zirconia oxygen sensor before and during oxidation experiment. Oxygen potential, which can be defined as $RT \ln P_{O_2}$ where R (J/mol/K) is the gas constant; T (K), the temperature and P_{O_2} (atm), the oxygen partial pressure, is shown for each experimental condition in Fig. 2, together with the standard Gibbs energies of formation for oxides oxygen potential of constituent elements of PNC316. As shown in this figure, almost all oxygen potentials in this experiment are lower than the standard Gibbs energy of formation of MoO_2. This means that the oxygen potential for each experimental condition was expected to be kept to be lower than that for MOX.

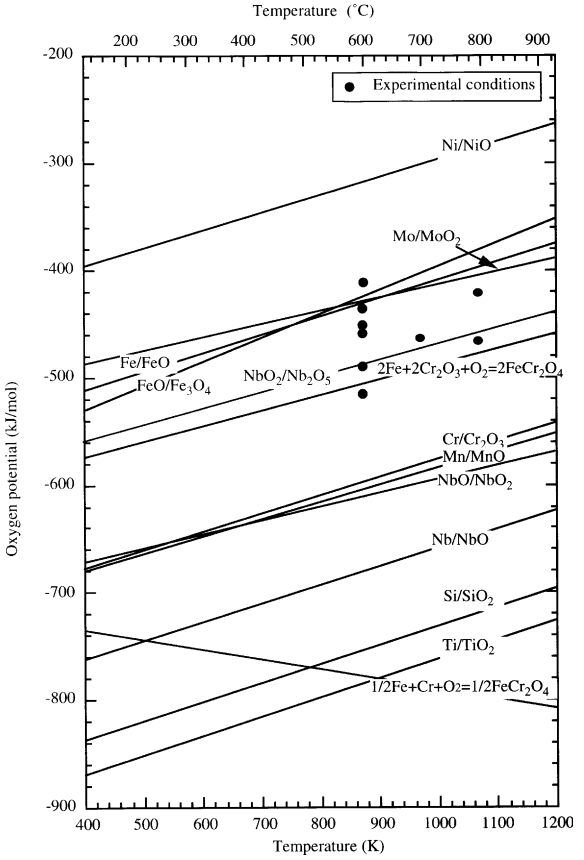

Fig. 2. Oxygen potential of the experimental atmosphere and standard Gibbs energies of formation for oxides of constituent elements of cladding materials.

This is because the standard Gibbs energy of formation of MoO_2 is comparable with that of MOX [2–4].

After the oxidation experiment, oxygen uptake of each specimen was measured using a carrier gas extract oxygen analyzer (EMGA-2200) with the error of $\pm 5.0 \times 10^{-4}$ mg/cm^2. This error resulted mainly from the statistical analysis and the calibration of oxygen analyzer. The oxidation products formed on the specimen surface were analyzed by using XRD. X-ray patterns from oxidized samples were acquired using an XD-D1 diffractometer by changing the incident angle of X-ray to the specimen surface in the range of 0.5–10°. This low incident angle method can clarify the distribution of products in the direction of depth from specimen surface. The diffractometer was used with Cu-Kα radiation and at conditions of 40 keV and 40 mA. Considering the absorption of Cu-Kα line by Fe elements in specimens, target of Co, Mo or Cr would be better for analysis of products including Fe element. However, difference in diffracted patterns from oxidized sample was found to be small on comparison between Cu- and Co-Kα radiations. Therefore, in this work, we discussed the XRD data obtained using Cu-Kα radiation.

In order to observe the structure of oxide layer and the distribution of elements therein, the cross-sections of oxidized samples embedded in an acrylic resin were observed examined with EPMA. The surfaces of the observed cross-sections were mechanically polished as described above. A part of specimens were etched with a solution of 75 vol.% HNO_3 and 25 vol.% H_2SO_4 to observe the effect of grain size on oxidation behavior.

3. Results

Fig. 3 shows oxygen uptakes by PNC316 and SUS316 as function of oxidation time at temperature of 600 °C under oxygen partial pressure of either 1.1×10^{-31}, 3.5×10^{-29} or 6.4×10^{-27} atm. The results obtained under these conditions indicated that the oxidation kinetics of PNC316 as well as SUS316 obeyed the parabolic rate law. Obviously, the oxygen uptake by both stainless steels increased with the oxygen partial pressure. And oxygen uptake by PNC316 was less than that of SUS316 other than the case for oxygen partial pressure of 6.4×10^{-27} atm.

For both PNC316 and SUS316, temperature dependence of oxidation kinetics is shown in Fig. 4. In this figure, oxygen uptake by PNC316 was less than that of SUS316 for all the experimental conditions. Ideally, in order to evaluate the temperature dependence of oxidation kinetics, oxygen partial pressure should be the same for every oxidation temperature. However, it was difficult to do so, and so, alternatively, the oxygen potential was kept to be the same value. In this figure, the

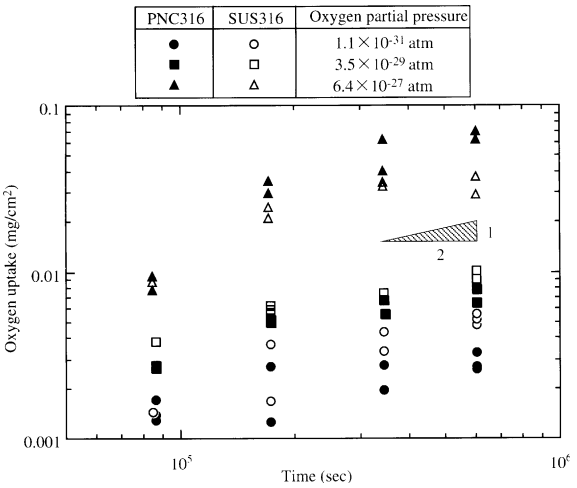

Fig. 3. Oxygen uptake as a function of reaction time at 600 °C under the oxygen partial pressures of 1.1×10^{-31}, 3.5×10^{-29} and 6.4×10^{-27} atm.

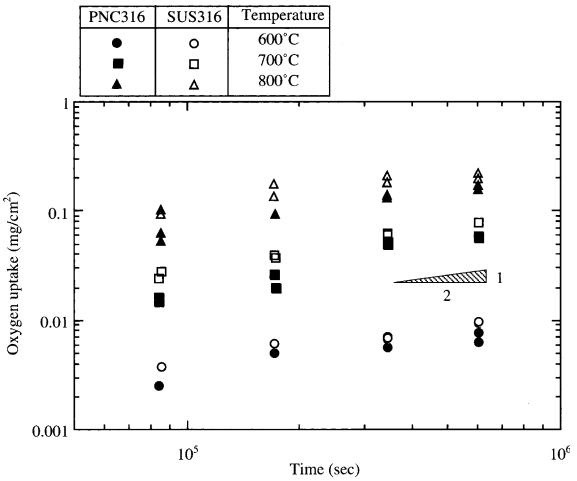

Fig. 4. Oxygen uptake as a function of reaction time at 600, 700 and 800 °C under the oxygen potential of -472 ± 4 kJ/mol.

oxygen potentials are shown to be equal to -472 ± 4 kJ/mol.

X-ray diffraction patterns of PNC316 specimen oxidized at 800 °C for 30 days under the oxygen partial pressure of 1.4×10^{-23} atm are shown in Fig. 5. Using the low incident angle method for XRD analysis, chemical forms of reaction layers on specimen surface can be determined in the direction of depth. The incident X-ray with the lower incident angle can pick up the more information from the outer layer near the atmosphere, while that with higher incident angle can do from the inner one near the interface between the reaction layer and the matrix metal. The diffraction pattern from the

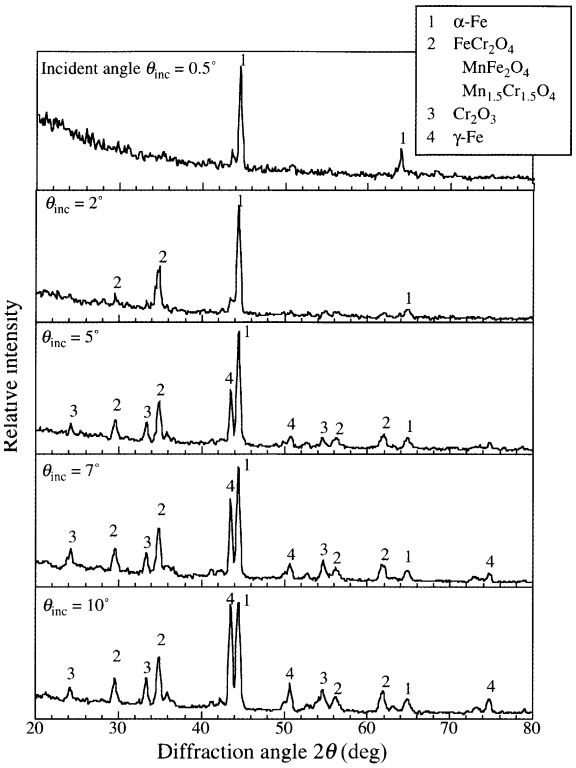

Fig. 5. X-ray diffraction patterns of PNC316 sample oxidized under the oxygen partial pressure of 1.4×10^{-23} atm at 800 °C for 30 days. XRD analysis was performed with X-ray incident angle between 0.5° and 10°.

outer layer indicates that this layer mainly consists of α-Fe (ferrite). On the other hand, results for higher incident angles show the patterns of Cr_2O_3, some multi-component oxides, α-Fe and γ-Fe (austenite). The γ-Fe phase has the lattice structure of the as-received PNC316 specimen.

Fig. 6 shows the results from EPMA for the oxidized specimen of PNC316 after exposure to oxygen partial pressure of 1.4×10^{-23} atm for 30 days at 800 °C. This specimen was exposed at a higher temperature and to a higher oxygen pressure comparing with the ones shown in Fig. 3. These conditions were adopted to get the thicker reaction layer appropriate for qualitative analyses. However, the oxidation mechanism of the specimen shown in Fig. 6 is supposed to be identical to that in Fig. 3 from the thermodynamical point of view. Fig. 6 illustrates that the reaction zone consists of two parts. The outer and inner layers consist of Fe–Ni and Cr–O (containing a small amount of Si), respectively. Fe and Ni cannot react with oxygen because of the high Gibbs energy of formation of these oxides. The reason why these elements existed in the outer layer is discussed below. On the other hand, Cr or Si preferentially reacts with oxygen to form oxides in the inner layers. As shown

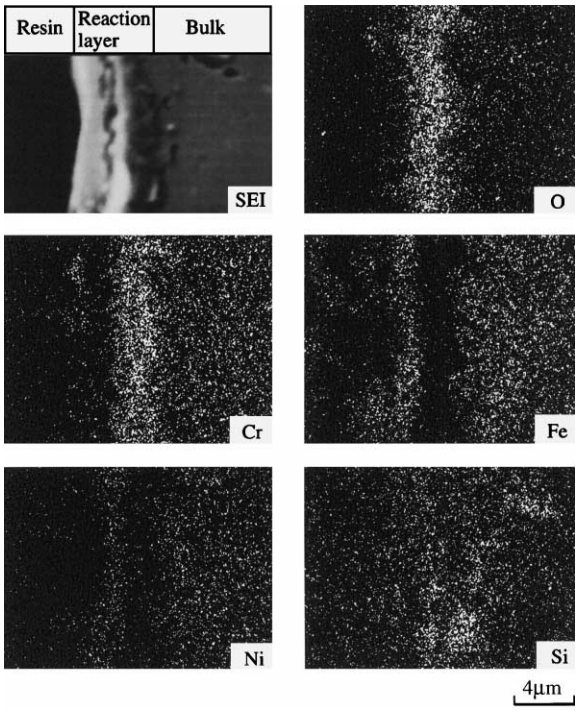

Fig. 6. EPMA analysis of cross-section of PNC316 after exposure to oxygen partial pressure of 1.4×10^{-23} atm at 800 °C for 30 days.

in Fig. 2, the oxygen potential for the present oxidation experiments was located between the Gibbs energy of formation of iron (or nickel) oxide (with one exception) and that of chromium (or silicon) oxide.

4. Discussion

Oxygen uptake by metals is described to increase parabolically, logarithmically, linearly or with other rate laws depending on oxide layer thickness [9]. For the stainless steels, the oxidation generally obeys the parabolic rate law when the thickness is μm order [9]. Furthermore, if the rate control process of oxidation is simply diffusion, oxygen uptake increases parabolically with time. As illustrated in Fig. 3, the oxidation of PNC316 and SUS316 proceeds obeying the parabolic rate law. In this work, the oxidation kinetics of both the stainless steels are assumed to be parabolic. The parabolic rate law is defined as

$$W^2 = k_p t, \tag{1}$$

where W is the oxygen uptake per unit area; k_p is a parabolic rate constant; t is the time.

Using the oxygen uptake data at 600 °C, the parabolic rate constants could be obtained fitting Eq. (1) to these data. The parabolic rate constants thus obtained are plotted as a function of oxygen partial pressure in Fig. 7. This figure also includes a result obtained by Saito using Mo/MoO_2 buffer [7]. The parabolic rate constant k_p of PNC316 was less than that of SUS316 in the range of the oxygen partial pressure from 10^{-31} to 10^{-27} atm. In addition, the k_p of PNC316 as well as of SUS316 increases with oxygen partial pressure.

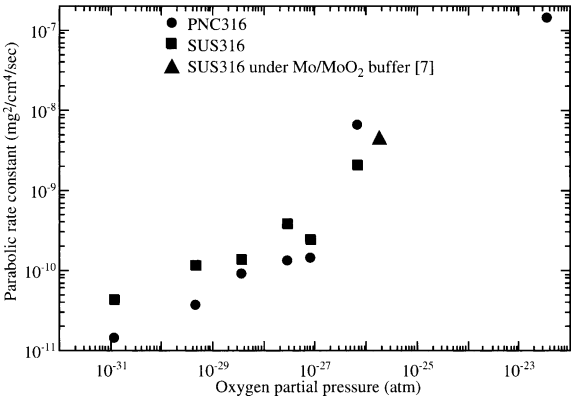

Fig. 7. Parabolic rate constants for PNC316 and SUS316 as a function of oxygen partial pressure at 600 °C.

In general, the rate constant of oxidation is dependent on oxygen partial pressure and temperature as the following equation:

$$k_p = k_0 \exp\left(-\frac{Q}{RT}\right) P_{O_2}^n, \tag{2}$$

where k_0 is the constant; Q is the activation energy. The power n is determined in the range of the oxygen partial pressure from 10^{-31} to 10^{-27} atm by using the data shown in Fig. 7. The values of n for PNC316 and SUS316 are obtained to be 0.279 and 0.313, respectively. Temperature dependences of the parabolic rate constant are shown in Fig. 8. Using Eq. (2) and obtained n values, activation energies for PNC316 and SUS316 are estimated to be 109 and 98 kJ/mol, respectively. Thus, the semi-empirical equations of the rate constant for PNC316 and SUS316 are respectively given by

$$k_p = 2.70 \times 10^4 \exp\left(-\frac{109}{RT}\right) P_{O_2}^{0.279} \tag{3}$$

and

$$k_p = 9.23 \times 10^4 \exp\left(-\frac{98}{RT}\right) P_{O_2}^{0.313}. \tag{4}$$

From the results of XRD and EPMA, oxides mainly consisting of Cr were observed on the surface of specimens in the range of the oxygen partial pressure from 10^{-31} to 10^{-27} atm. Fig. 2 shows that the added elements other than Fe, Ni and Mo can be thermochemically

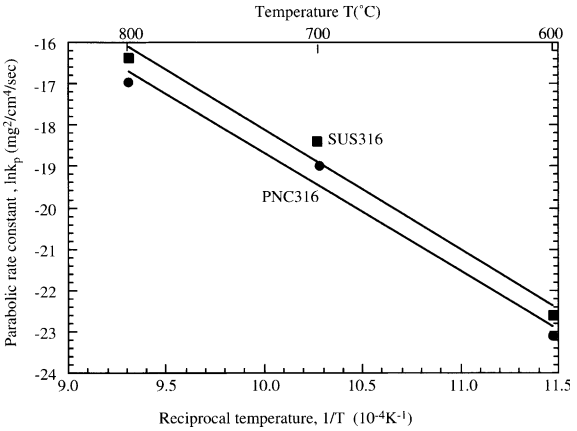

Fig. 8. Parabolic rate constants as a function of $1/T$ under the oxygen potential of -472 ± 4 kJ/mol.

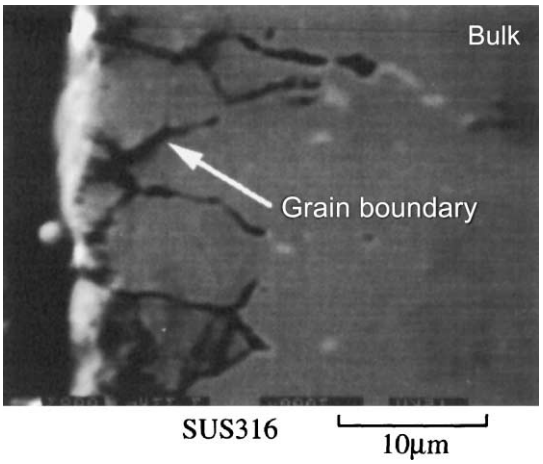

Fig. 9. Comparison of oxidation layers on PNC316 (see Fig. 6) and SUS316. Both samples were oxidized under the oxygen partial pressure of 1.4×10^{-23} atm at 800 °C for 30 days.

oxidized under the above-described low oxygen partial pressure. Here, assuming that oxidation rate for both stainless steels is controlled by Cr diffusion in Cr_2O_3 layer, oxygen partial pressure dependence of oxidation rate is discussed as follows. When the pure Cr metal is oxidized, the Cr_2O_3 formed on a specimen has non-stoichiometry of metal-deficient type. Ionized Cr vacancies may arise according to

$$3/2O_2 = 2V'''_{Cr} + 6h^{\bullet} + 3O^{\times}_{O}, \tag{5}$$

where V'''_{Cr} is the Cr vacancy; $h^{\bullet}$ is the hole; $O^{\times}_{O}$ is the oxygen on a regular site [10]. Applying the mass-action law to Eq. (5) under the assumption that the oxidation rate is proportional to concentration of Cr vacancies, relation between k_p and oxygen partial pressure is given by

$$k_p \propto P_{O_2}^{3/16}. \tag{6}$$

The values of power of oxygen partial pressure were 0.279 and 0.313 for PNC316 and SUS316, respectively. The difference between the experimentally obtained values and the theoretical one of 0.188 ($= 3/16$) can be attributed to oversimplified rate control process of diffusion for oxidation. In the oxidation experiments under the low oxygen partial pressure, Si and Mn as well as Cr were oxidized as shown in Figs. 5 and 6. In addition, a minor amount of Fe might be oxidized to form a complex oxide with Cr. The activation energies shown in Eqs. (2) and (3) were 109 and 98 kJ/mol for PNC316 and SUS316, respectively. In the case of oxidation of pure Cr metal, the activation energy is reported to be about 230 kJ/mol [11], much larger than the values obtained in this work. However, the former values agree with that of 100 kJ/mol evaluated by Saito et al. [7]. In their report, diffusion of Cr in oxide layers is considered to be rate control process of oxidation of stainless steels. These lower activation energies for stainless steel may result not only from the effect of alloying but also from geometrical effect, e.g. grain size.

Fig. 9 shows the cross-sectional view of a SUS316 sample oxidized at 800 °C for 30 days under 1.4×10^{-23} atm of the oxygen partial pressure. As seen in Figs. 6 and 9, both PNC316 and SUS316 specimens showed that oxidation took place along grain boundaries as well as on the surface. PNC316 exhibits better oxidation resistance along grain boundaries. The grain sizes of as-received PNC316 and SUS316 were ~40 and ~20 μm, respectively. In order to know the effect of grain boundaries on oxidation, the oxidation experiment was performed using the PNC316 specimens annealed in vacuum at 1100 °C for 4 h. The grain size of specimens after this heat treatment was ~150 μm. Comparing the oxidation of both as-received and heat treated PNC316, less oxygen uptake was measured for heat treated specimens than as-received ones (Table 2). EPMA examinations indicated that oxides along grain boundaries included a large amount of Cr and Si. Therefore, the large grain size is one of the reasons for the better oxidation resistance of PNC316.

Table 2
Effect of grain size on oxidation of PNC316

Grain size (μm)	Oxygen uptake (mg/cm^2)
40	0.0075
150	0.0050

Oxidation experiment was performed under the oxygen partial pressure of 7.2×10^{-28} atm at temperature of 600 °C for four days.

PNC316 contains small amount of Ti and Nb. These minor added elements can form carbides like Cr. In terms of standard Gibbs energy of formation of these carbides, TiC and NbC are more stable than $Cr_{23}C_6$. Under the low oxygen partial pressure of this work, Cr prefers to be formed in the form of oxide rather than carbide. Part of chromium carbide in the specimen was oxidized according to the following reaction which occurs preferably along grain boundaries:

$$2/23Cr_{23}C_6 + 3/2O_2 = Cr_2O_3 + 12/23C. \quad (7)$$

For PNC316 specimens, Ti and Nb may suppress the formation of chromium carbide, and consequently, oxidation of Cr through the reaction (7) may be suppressed. Therefore, addition of Ti and Nb most probably causes less oxygen uptake by PNC316 than that of SUS316.

The oxidation rate constants of PNC316 and SUS316 at the vicinity of oxygen partial pressure of 1×10^{-26} atm are much larger than those obtained under the lower oxygen partial pressures as shown in Fig. 7. This oxygen partial pressure is almost equal to the equilibrium oxygen partial pressure of Fe–FeO system at 600 °C. The large increase of rate constant is the reason why iron oxides, e.g. FeO, Fe_3O_4, are formed together with oxides formed under the lower oxygen partial pressure, e.g. Cr_2O_3, $FeCr_2O_4$ and so on. Furthermore, Fig. 7 shows that the rate constant of PNC316 at this particular oxygen partial pressure is larger than that of SUS316. In such a case, iron oxides formed at higher oxygen partial pressure are observed in the outer layer of duplex oxide layer [12]. In the inner layer, chromium oxides are mainly observed [12]. The iron oxides cannot be formed just on the grain boundaries of specimens since chromium oxides were precedently formed at grain boundaries. Therefore, the rate constant of PNC316, of which grain size is large, is larger than that of SUS316.

Fig. 10 shows an EPMA line analysis for surface of an oxidized specimen of PNC316 at 600 °C for seven days under oxygen partial pressure of 7.6×10^{-28} atm. For these metallic precipitates, intensity of characteristic X-ray from Fe is strong, but ones from Cr and O are weak. Under the low oxygen partial pressure, such metallic precipitates are usually observed. Therefore, it is reasonably figured out that the number of these precipitates increases as passing oxidation time, and consequently, the layer including Fe and Ni is formed on the outer part of the reaction layer (Fig. 6). In order to explain the oxidation kinetics of PNC316, we assumed that Cr diffusion in the Cr_2O_3 layer controlled its kinetics. As shown in Fig. 5, multicomponent oxides, e.g. $FeCr_2O_4$, as well as Cr_2O_3 existed in the inner reaction layer. In terms of the Gibbs energy of formation of oxide, the $FeCr_2O_4$ layer might be formed on the Cr_2O_3 layer. Assuming that, in the Cr_2O_3 layer, Fe as well as Cr

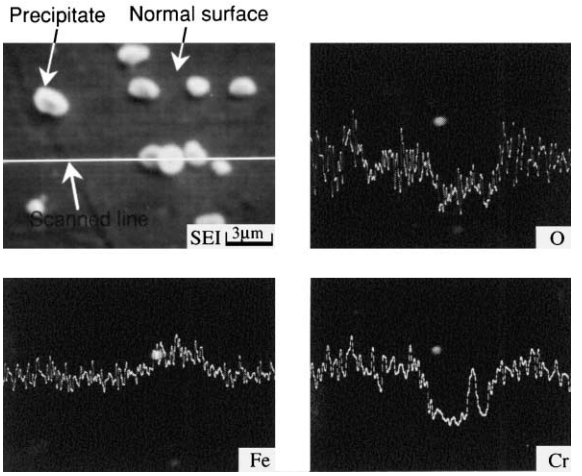

Fig. 10. EPMA line analysis for precipitates on surface of PNC316 samples oxidized under the oxygen partial pressure of 7.6×10^{-28} atm at 600 °C for seven days.

diffuses fast and that, in the $FeCr_2O_4$ layer, O diffuses fast, Fe can precipitate in the most outer layer. However, the diffusion coefficient of O is known to be relatively large in the α-Fe [13], but that in the $FeCr_2O_4$ has not been clearly understood so far.

In XRD analysis, α-Fe was detected as the outer layer on the oxide layer formed under the low oxygen partial pressure. Formation of such layers, in which iron oxides were not included, had not been reported. According to the phase diagram of Fe–C [14], α-Fe includes little carbon (<0.02%) and stably exists below the temperature of 910 °C. As a result, α-Fe may be formed by the annealing effect during the oxidation experiment. However, as shown in Fig. 6, the layer of which the lattice structure is α-Fe phase includes Ni nearly in proportion to its original concentration (Table 1). And Ni added to stainless steels can stabilize the γ-Fe phase [14]. Even if the depletion of Cr is caused by oxidation, a little amount of Cr still exists in the outer layer. Therefore, taking into account a certain amount of Ni and Cr coexisting in the outer layer, change from γ- to α-Fe phase may be hard at the temperature of greater than ~700 °C. As discussed above, the mechanism of occurrence of α-Fe phase seems to be complicated. In order to understand such phenomena fully, more detailed analyses are needed.

This work reveals that metallic Fe precipitates are formed at the top of the oxide layer under the low oxygen potential, and suggests that Fe probably covers the cladding inner surface in the first stage of irradiation, where the amount of corrosive FPs are not enough to attack the cladding. A previous report indicates that the cladding material oxidized under low oxygen potential to form a protective oxidation layer was found to be

superior to fresh ones in resistance against attack by Te [15]. Therefore, it is possible to imagine that the existence of the metallic Fe precipitates has some effect on the quantity and feature of FCCI when corrosive FPs accumulating at the fuel cladding gap attack the inside of cladding at higher burn-up. For evaluation of oxidation mechanism and oxidation rate of the cladding, it is highly important to consider the reaction to occur at the initial stage of irradiation (under low oxygen potential).

5. Conclusion

The oxidation behaviors of PNC316 as well as SUS316 were systematically evaluated in terms of dependencies on oxygen partial pressure, temperature and time under the low oxygen partial pressure. In this work, the oxygen partial pressure was controlled by changing the ratio of pressures of H_2 and H_2O gas components in Ar carrier gas. As a result, the following results were obtained.

(1) Oxygen uptake by these cladding materials increased parabolically with time, and the obtained kinetic constants were dependent on both oxygen partial pressure and temperature. Semi-empirical equation of the parabolic rate constant for each material was $2.70 \times 10^4 \exp(-109/RT)P_{O_2}^{0.279}$ for PNC316 and $9.23 \times 10^4 \exp(-98/RT)P_{O_2}^{0.313}$ for SUS316.
(2) Oxygen uptake by PNC316 was less than that of SUS316 under the low oxygen partial pressure, which might result from the effect of larger grain size and alloying addition of Ti and Nb for PNC316. These additive elements could suppress the production of chromium carbide, $Cr_{23}C_6$, which would be easily oxidized to form the oxide.
(3) The duplex layers were observed on the samples oxidized under the low oxygen partial pressure. The inner layer consisted of multiple phase oxides such as Cr_2O_3, complex oxides and SiO_2. On the other hand, the outer layer mainly consisted of α-Fe. The α-Fe thus observed may play an important role in the attack by corrosive FPs at high burn-up.

Acknowledgements

The authors are grateful to K. Mori for allowing use of oxygen analyzer and also to M. Watanabe of the Center of Advanced Instrumental Analysis, Kyushu University, for her help with the X-ray diffraction measurements. They also wish to thank the technical staffs, M. Kutsuwada and K. Wakasugi.

References

[1] M. Hori, T. Fukuda, T. Takahashi, Proc. Int. Conf. on Fast Reactor and Related Fuel Cycle (FR '91), Kyoto, Japan, October 28–November 1, vol. 1, 1991, p. 5.
[2] R.E. Woodley, J. Nucl. Mater. 96 (1981) 5.
[3] Hj. Matzke, J. Ottaviani, D. Pellottiero, J. Rouault, J. Nucl. Mater. 160 (1988) 142.
[4] I. Sato, H. Furuya, K. Idemitsu, T. Arima, K. Yamamoto, M. Kajitani, J. Nucl. Mater. 247 (1997) 46.
[5] M.J. Bennett, M.R. Houlton, J. Nucl. Mater. 71 (1978) 333.
[6] T. Noda, M. Okada, R. Watanabe, J. Nucl. Sci. Technol. 17 (1980) 191.
[7] M. Saito, Y. Ishikawa, K. Ikeda, H. Furuya, J. Nucl. Sci. Technol. 21 (1984) 356.
[8] I. Shibahara, S. Ukai, S. Onose, S. Shikakura, J. Nucl. Mater. 204 (1993) 131.
[9] T. Mori, Science of Steel Crossion, Asakurashoten, 1976 (in Japanese).
[10] P. Kofstad, K.P. Lillerud, J. Electrochem. Soc. 127 (1980) 2410.
[11] K.P. Lillerud, P. Kofstad, Oxidat. Met. 17 (1982) 127.
[12] M. Saito, H. Furuya, M. Sugisaki, J. Nucl. Mater. (1985) 11.
[13] A.K. Stewart, M.T. Hepworth, Trans. Metall. Soc. AIME 242 (1968) 698.
[14] R.P. Elliott, Constitution of Binary Alloys (First supplement), McGraw-Hill, New York, 1965.
[15] I. Sato, T. Arima, K. Idemitu, K. Yamamoto, T. Namekawa, JNC TY9400 99003 (in Japanese).